**X. H. Shen**
School of Aeronautics and Astronautics,
Purdue University,
West Lafayette, IN 47907;
Department of Mechanical and
Aerospace Engineering,
University of Missouri,
Columbia, MO 65211

**C. T. Sun**
School of Aeronautics and Astronautics,
Purdue University,
West Lafayette, IN 47907

**M. V. Barnhart**
Department of Mechanical and
Aerospace Engineering,
University of Missouri,
Columbia, MO 65211

**G. L. Huang**[1]
Department of Mechanical and
Aerospace Engineering,
University of Missouri,
Columbia, MO 65211
e-mail: huangg@missouri.edu

# Analysis of Dynamic Behavior of the Finite Elastic Metamaterial-Based Structure With Frequency-Dependent Properties

*For practical applications of the elastic metamaterials, dynamic behavior of finite structures made of elastic metamaterials with frequency dependent properties are analyzed theoretically and numerically. First, based on a frequency-dependent mass density and Young's modulus of the effective continuum, the global dynamic response of a finite rod made of elastic metamaterials is studied. It is found that due to the variation of the effective density and Young's modulus, the natural frequency distribution of the finite structure is altered. Furthermore, based on the spectral approach, the general wave amplitude transfer function is derived before the final transmitted wave amplitude for the finite-layered metamaterial structure with decreasing density is obtained using the mathematical induction method. The analytical analysis and finite element solutions indicate that the increased transmission wave displacement amplitude and reduced stress amplitude can be controlled by the impedance mismatch of the adjacent layers of the layered structure*. [DOI: 10.1115/1.4038950]

## 1 Introduction

Liu et al. fabricated the first artificial metamaterial capable of generating a negative effective mass near the resonant frequency of substructures made of rubber-coated lead (Pb) spheres [1]. Since then, researchers have focused on elaborating on the physical meaning of the negative effective mass phenomenon [2–6], as well as designing new types of acoustic/elastic metamaterials with negative effective mass and/or negative effective modulus [7,8]. Recently, the realization of metamaterials with a near-zero-index has become the subject of increasing interest [9–12]. This shift to non-negative material properties opens a new chapter of metamaterial research, which expands the definition of metamaterials to a material with "on-demand" effective properties without the constraints imposed by what nature provides [13–15].

In the past, layered structures have demonstrated the ability to achieve vibration isolation and reduce the overall stress amplitude of dynamic disturbances [16,17]. The earliest theoretical discussions for wave propagation in media consisting of a number of elastic layers can be traced back to Thomson's derivation in 1950 [18], which introduced the transfer matrix approach in the time domain to relate the displacements and stresses at the bottom of a layer to those at its top. Due to the complexity of wave propagation in finite layered structures, frequency domain approaches have recently been proposed to perform analysis and determine optimal designs of layered structures [16,17]. However, it is extremely difficult to find suitable natural materials for the multilayered structures to actually control the displacement and stress transmission amplitudes quantitatively, due to the limitation of their inherent properties. On the other hand, elastic metamaterials can deliver any desired dynamic mass density and/or Young's modulus by controlling the wave frequency. This is much more efficient when constructing layered structures capable of controlling wave propagation characteristics. Recently, Srivastava and Willis studied out-of-plane wave propagation toward the interface between a finite layered medium and its homogeneous medium [19]. It was found that the evanescent waves from boundary layers should be considered to meet continuous conditions of the displacement and stress fields.

Due to the catastrophic effect, vibration and mechanical resonance is a significant problem in industry. Within the band gap, resonant-based metamaterials could provide a solution for subwavelength vibration isolation and/or absorbing unwanted noise, which can be interpreted by the frequency-dependent properties. It is well known that the unnatural mechanical properties inherent to elastic/acoustic metamaterial, including negative effective mass, negative effective modulus, and near-zero mass density, originate from its internal structure. Therefore, elastic metamaterials can be designed to have any mass density or modulus by simply changing its internal microstructure. However, much less attention has been paid on the dynamic behavior of the metamaterials within the passing band especially when the structure is in a finite length. It can be anticipated that the global dynamic spectrum behavior of the finite metamaterial-based structure will be altered due to the embedded microstructures and cannot simply captured by using the simple Cauchy medium. To fill this gap and elucidate the influence of the frequency-dependent properties on the natural frequency of the finite structure, the dynamic response of the finite metamaterial-based structure with frequency dependent properties is analyzed analytically and numerically.

In this paper, spectrum and vibration analysis of finite elastic metamaterial-based rod is performed analytical and numerically to illustrate the effects of the frequency-dependent properties on the resonate frequency of the finite structure. Then, the spectral approach [16,17,20,21] is utilized and the transfer function for the general wave amplitudes is derived for wave propagation in the

[1]Corresponding author.
Contributed by the Technical Committee on Vibration and Sound of ASME for publication in the Journal of Vibration and Acoustics. Manuscript received June 27, 2017; final manuscript received January 4, 2018; published online February 9, 2018. Assoc. Editor: Mahmoud Hussein.

  

finite metamaterial-based layered structure. Finally, the transmitted wave amplitude and its range for one special case in which a layered structure comprised of continuum media with decreasing density is studied.

## 2 Effective Mass and Young's Modulus of Metamaterials in Lattice Form

A common approach to model an infinite discrete metamaterial is to use a lattice system of mass-spring units [2–6]. An example of this modeling approach is shown in Fig. 1, which depicts a one-dimensional (1D) mass-in-mass lattice system where each unit cell in the lattice is arranged at a distance, $d$, from its neighboring cell [5].

To describe the behavior of a harmonic wave propagating through the lattice system, the equations of motion for the $j$th unit are obtained as

$$m_1^{(j)}\frac{d^2u_1^{(j)}}{dt^2}+k_1\left(2u_1^{(j)}-u_1^{(j-1)}-u_1^{(j+1)}\right)+k_2\left(u_1^{(j)}-u_2^{(j)}\right)=0 \tag{1a}$$

$$m_2^{(j)}\frac{d^2u_2^{(j)}}{dt^2}+k_2\left(u_2^{(j)}-u_1^{(j)}\right)=0 \tag{1b}$$

where $u_\gamma^{(j)}$ denotes the displacement of mass "$\gamma$" ($=1, 2$) in the $j$th unit cell of the lattice. Similarly, for the $(j+n)$th unit cell, the harmonic displacement is expressed as

$$u_\gamma^{(j+n)}=A_\gamma e^{i(nqd-\omega t)} \tag{2}$$

where $A_\gamma$ is the wave amplitude, $q$ is the wavenumber, and $\omega$ is the angular frequency.

Substituting Eq. (2) into Eq. (1) yields two homogeneous equations for $A_1$ and $A_2$, from which the dispersion relation is obtained as the determinant of the coefficient matrix

$$m_1m_2\omega^4-[(m_1+m_2)k_2+2m_2k_1(1-\cos(qd))]\omega^2+2k_1k_2(1-\cos(qd))=0 \tag{3}$$

The mass-in-mass system could be further represented as a monatomic lattice with a single effective mass as shown in Fig. 2.

For the effective monatomic mass-spring lattice system shown in Fig. 2, the equation of motion for the $j$th unit cell is written as

$$m_{\text{eff}}^{(j)}\frac{d^2u^{(j)}}{dt^2}+k_1(2u^{(j)}-u^{(j-1)}-u^{(j+1)})=0 \tag{4}$$

Following the harmonic solution, the displacement of the $(j+n)$th unit cell is written as

$$u^{(j+n)}=A_{\text{eff}}e^{i(nqd-\omega t)} \tag{5}$$

Substituting Eq. (5) into Eq. (4), the dispersion relation for this effective monatomic lattice system is obtained as

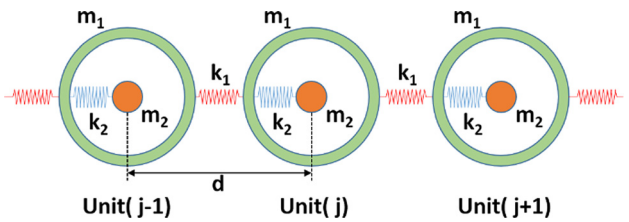


**Fig. 1 Infinite mass-in-mass lattice model**

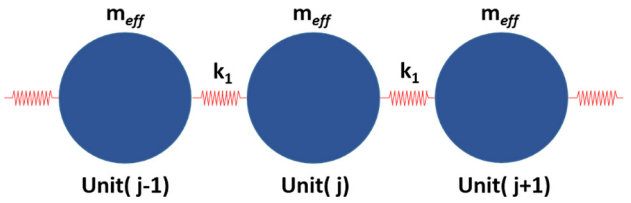


**Fig. 2 Infinite effective mass lattice model**

$$m_{\text{eff}}\omega^2=2k_1(1-\cos(qd)) \tag{6}$$

Since the dispersion curves of the effective system should be identical to the equivalent mass-in-mass lattice representation, equating Eq. (3) with Eq. (6) leads to

$$m_{\text{eff}}=\frac{(m_1+m_2)k_2-m_1m_2\omega^2}{k_2-m_2\omega^2} \tag{7}$$

The next step is to homogenize the effective monatomic mass lattice model into its corresponding continuum representation [5,6,22]. The representative unit cell in Fig. 2 can be represented as two masses connected by a spring shown in Fig. 3.

If a symmetric pair of harmonic forces of the form $F=\hat{F}e^{i\omega t}$ are applied to the representative unit cell, the equation of motion can then be obtained as

$$F=2k_1u+\frac{1}{2}m_{\text{eff}}\frac{\partial^2u}{\partial t^2} \tag{8}$$

Substituting the harmonic displacement $u=\hat{u}e^{i\omega t}$ into Eq. (8), we can readily obtain the relation between the applied forces and effective mass displacement as

$$\hat{F}=\left(2k_1-\frac{1}{2}m_{\text{eff}}\omega^2\right)\hat{u} \tag{9}$$

Considering the effective continuum model shown in Fig. 3, its stress–strain relation is given by

$$\hat{\sigma}=E_{\text{eff}}\hat{\varepsilon} \tag{10}$$

where the average stress and strain are, respectively, calculated as $\hat{\sigma}=\hat{F}/A$ and $\hat{\varepsilon}=2\hat{u}/d$, where $d$ is the unit cell size, $E_{\text{eff}}$ is the effective Young's modulus of the 1D continuum model, and $A$ is the cross-sectional area of the continuum model. Substituting Eq. (9) into Eq. (10) and normalizing with respect to the static Young's modulus $E_{\text{st}}=k_1d/A$, the ratio of effective and static moduli can be obtained as

$$\frac{E_{\text{eff}}}{E_{\text{st}}}=1-\frac{1}{4}\frac{m_{\text{eff}}}{k_1}\omega^2 \tag{11}$$

Based on Eqs. (4), (7), and (11), Fig. 4 shows the dispersion curves, effective mass, and effective Young's modulus for the material constants $\theta=m_2/m_1=0.5$, $\delta=k_2/k_1=0.8$, and local resonance frequency $\omega_0=\sqrt{k_2/m_2}=20$ (rad/s). The resulting band gap corresponds to both the negative effective mass and negative effective Young's modulus frequency regions. It is clear that the local resonance frequency, $\omega_0$, is the cause of the negative effective material properties which is expected.

## 3 Influence of Frequency-Dependent Properties on Rod Vibrations

Unlike the constant physical properties of materials used in conventional structures, the effective mass density and Young's modulus of a structure made of metamaterials are highly

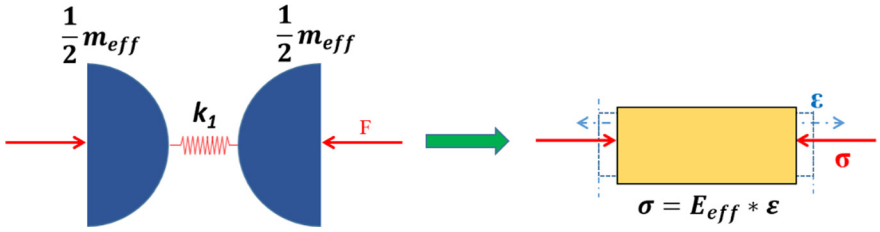


**Fig. 3 Unit cell of monatomic effective mass lattice model (left) and effective continuum representation (right)**

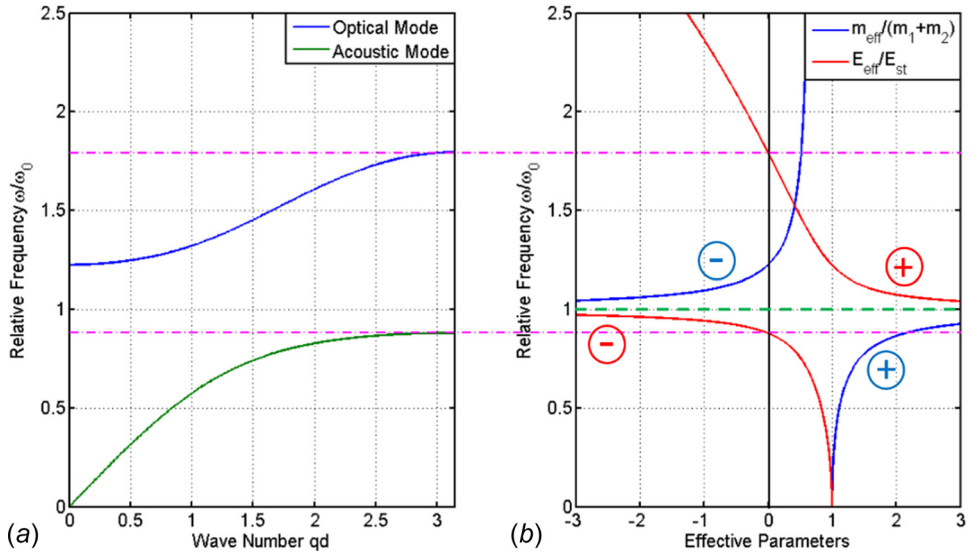


**Fig. 4 (*a*) Dispersion curves of lattice system and (*b*) effective mass and Young's modulus parameters**

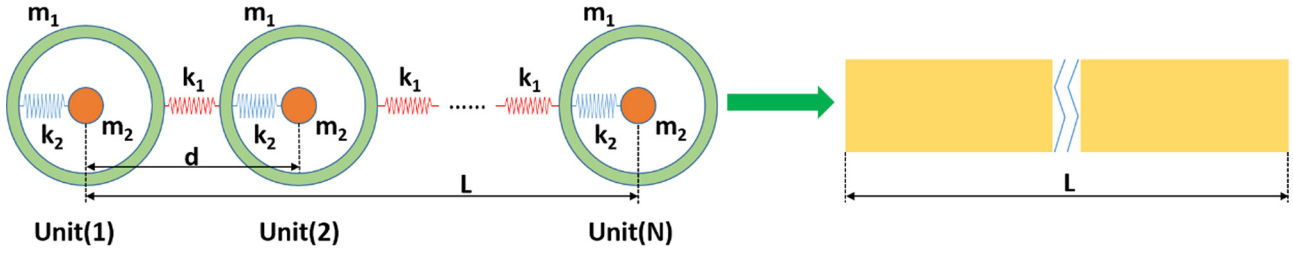


**Fig. 5 Finite mass-in-mass lattice model and analogous effective continuum rod (free-free boundary condition)**

dependent on the excitation frequency applied. Although metamaterial substructures (unit cells) have been designed to tune the overall structural stiffness [14] or to isolate dynamic disturbances [15], the dynamic response of a structure using metamaterials as structural building blocks is still an unelucidated problem to the best of our knowledge. To study this problem, the vibration response of a metamaterial rod is analyzed in this section.

**3.1 Analytical Analysis of Dynamic Behavior in Finite Elastic Metamaterial Rod.** The finite mass-in-mass lattice model and corresponding continuum model that will be analyzed are shown in Fig. 5. The cross-sectional area of the rod is denoted by $A$, and its total length as $L$. Based on Hamilton's principle and the assumption that no damping is present in the structure, the governing equation of motion of the continuum rod can be expressed as

$$\frac{\partial}{\partial x}\left[EA\frac{\partial u}{\partial x}\right] - \rho A\frac{\partial^2 u}{\partial t^2} = 0 \tag{12}$$

For harmonic motions, the displacement is [20]

$$u(x,t) = \hat{u}(x,\omega)e^{i\omega t} \tag{13}$$

Substituting Eq. (13) into Eq. (12), we obtain the displacement solution in the form

$$\hat{u}(x) = C_1 e^{ikx} + C_2 e^{-ikx}, \quad k^2 = \frac{\rho_{\text{eff}}}{E_{\text{eff}}}\omega^2 = \frac{m_{\text{eff}}}{E_{\text{eff}} \cdot A \cdot d}\omega^2 \tag{14}$$

where $\rho_{\text{eff}} = m_{\text{eff}}/Ad$.

If the angular wave frequency, $\omega$, is within the band gap frequency region, either the effective mass or the effective Young's modulus will become negative. Based on Eq. (14), the negative effective parameters result in a purely imaginary wave number such that $k = i\alpha$, where $\alpha$ is a real number. Thus, Eq. (14) can be rewritten as Eq. (15), and the solution from Eq. (15) can be interpreted as either the left-to-right ($C_1 e^{-\alpha x}$) or right-to-left ($C_2 e^{\alpha x}$) directions of the traveling incident or reflected wave [20],

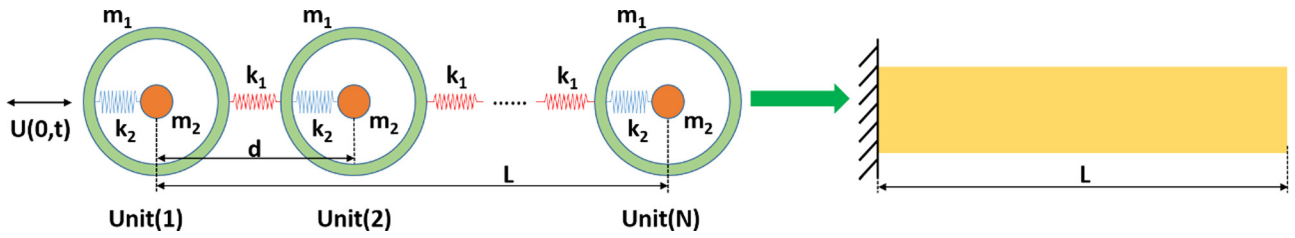


**Fig. 6 Finite mass-in-mass lattice model and effective continuum rod (fixed-free end)**

respectively. When the incident wave is superimposed on the reflected wave traveling in the opposite direction, both waves' displacement amplitudes monotonically decrease along the propagation direction exponentially. It is apparent that for any boundary conditions, such as free-free end and fixed-free end, only a trivial solution can be obtained from Eq. (15), which indicates that there is no natural resonance frequency in the band gap frequency region

$$\hat{u}(x) = C_1 e^{-\alpha x} + C_2 e^{\alpha x} \tag{15}$$

Outside the band gap frequency region, however, the wave number is a real number and the displacement is in the form

$$\hat{u}(x) = c_1 \cos(kx) + c_2 \sin(kx) \tag{16}$$

Considering free vibration of the rod with a free-free boundary condition as shown in Fig. 5, the resonance frequencies can be expressed as

$$\omega_n = \frac{n\pi}{L}\sqrt{\frac{E_{\text{eff}}}{\rho_{\text{eff}}}}, \quad n = 0, 1, 2, \ldots \tag{17}$$

It should be noted that in Eq. (17), the effective Young's modulus and mass density are both frequency dependent. Thus, the physical meaning of $\sqrt{E_{\text{eff}}/\rho_{\text{eff}}}$ is the resonance frequency for the rod under a certain frequency excitation, and its effective mechanical properties are also frequency dependent. Substituting Eqs. (7) and (11) into Eq. (17), the resulting resonance frequencies should satisfy the relation

$$\begin{aligned} &m_1 m_2 (4L^2 + n^2\pi^2 d^2)\omega_n^4 \\ &\quad - [4m_2 n^2\pi^2 d^2 k_1 + (m_1 + m_2)(4L^2 + n^2\pi^2 d^2)k_2]\omega_n^2 \\ &\quad + 4n^2\pi^2 d^2 k_1 k_2 = 0 \end{aligned} \tag{18}$$

From Eq. (18), it is found that for each $n$, there are two sets of unique resonance frequencies. For the first mode in each set, the two solutions can be obtained from Eq. (19) below. Compared with Eq. (7), it is easy to see that the effective mass is zero at $\omega_2$, which corresponds to the upper frequency cutoff for the band gap shown in Fig. 4

$$\omega_1 = 0, \quad \omega_2 = \frac{k_2(m_1 + m_2)}{m_1 m_2} \tag{19}$$

For the high-order modes ($n \to \infty$), the resonance frequency can be obtained from Eq. (20). Compared with Eq. (11), it is easy to see that the effective Young's modulus is zero at two solutions of $\omega_\infty$, which correspond to the two lower cutoff frequencies of the band gap shown in Fig. 4

$$(\omega_\infty)^2 = \frac{[(m_1 + m_2)k_2 + 4k_1 m_2] \pm \sqrt{(m_1 + m_2)^2 k_2^2 + 16k_1^2 m_2^2 + 8k_1 k_2 m_2 (m_2 - m_1)}}{2m_1 m_2} \tag{20}$$

For free vibrations of the finite rod with a fixed-free boundary condition as shown in Fig. 6, the parameter $n$ in Eqs. (17) and (18) needs to be replaced by $n + (1/2)$, but for the high-order modes ($n \to \infty$), the form of the resonance frequencies remains the same as in Eq. (20).

Comparing Eqs. (17) and (20), it can be found that for a conventional continuum rod, the high-order resonance frequency approaches infinity. However, for the rod made of elastic metamaterials, the resonance frequency converges to a finite value. When conducting vibrational analysis, this characteristic will influence the natural frequency distribution of structures made of elastic metamaterials, which is demonstrated in Sec. 3.2.

**3.2 Numerical Simulation of Dynamic Behavior in Finite Elastic Metamaterial Rod.** Based on Eq. (15), there should be no natural resonance frequency located in the band gap frequency region. To verify this analytical solution, Fig. 7 compares the dispersion curve calculated with Eq. (3) with the natural resonance frequency calculated with Eq. (18), for the specific set of material constants: $\theta = m_2/m_1 = 0.5$, $\delta = k_2/k_1 = 0.8$, $d = 1$ m, $L = 100$ m and $\omega_0 = \sqrt{k_2/m_2} = 20$ (rad/s). It is obvious that there is no resonance frequency (Fig. 7(*b*)) within the band gap frequency region (Fig. 7(*a*)), and as predicted in Sec. 3.1, $\omega_2$ and $\omega_\infty$ define the upper and lower bounds of the band gap, respectively.

Figure 8 shows the free-free boundary condition for the mass-in-mass lattice model with the same set of material constants used in Fig. 7.

Using the analytical solution obtained from Eq. (18) and the numerical solution obtained using ABAQUS, the two sets of natural resonance frequency of metamaterial rod can be compared as shown in Fig. 9. It should be noted that the natural frequencies obtained from the two approaches start and end (dashed line) at the same frequencies, which verifies that no resonant frequency is present within the band gap region for either solution. In addition, it is also noted that the analytical and finite element method solutions are in good agreement for the frequency regions with a small mode number but begin to diverge for higher modes. This is caused by the finite number of resonators considered in the numerical model, which cannot obtain the infinite number of modes obtained analytically with Eq. (18). Comparing the resonance

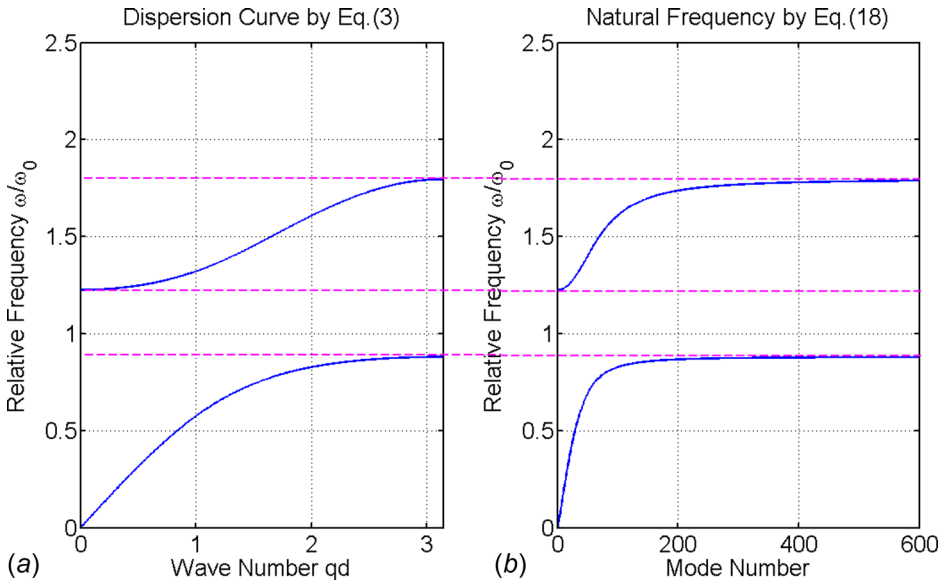


**Fig. 7 Comparison of (*a*) dispersion curves with band gap and (*b*) natural frequencies of metamaterial rod**

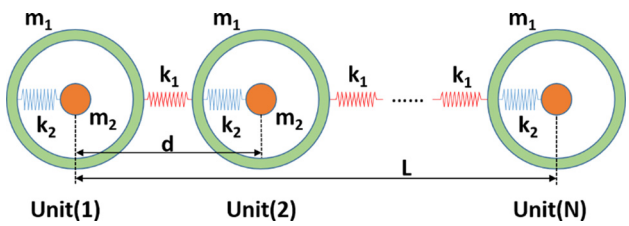


**Fig. 8 Free–free boundary condition of finite mass-in-mass lattice model in ABAQUS**

frequencies obtained for the finite elastic metamaterial rod with 100 and 20 resonators shown in Fig. 9, it is clear that if more resonators are considered in the finite elastic metamaterial rod, more modes can be observed.

In Fig. 10, the mass-in-mass lattice model and its effective continuum rod with a prescribed displacement as input are created in ABAQUS. The material constants are the same as those used in Fig. 7, except now $L = 20$ m.

To show the difference in the natural frequency distribution, Fig. 11 compares the steady-state displacement of the remote end of the conventional material rod with the last unit cell's outer mass, $m_1$, of the elastic metamaterial rod. The mass density and Young's modulus of the conventional material rod are $\rho = 63\,\text{kg/m}^3$ and $E = 10{,}000\,\text{Pa}$, respectively. The obvious band gap in Fig. 11(*a*) indicates that the resonators inside the rod can significantly isolate the vibration. Furthermore, as shown in Fig. 11(*b*), due to the variation of the effective mass density and Young's modulus, the rod's resonance frequency distribution is altered, especially in the frequency region close to the local resonance frequency of the unit cells' internal resonator, $m_2$. This interesting phenomenon requires special attention because the resonance frequency concentration below and above the band gap will amplify the input force/displacement instead of attenuating it.

## 4 Wave Propagation in Finite Layered Structures

Due to the wide technological applications, layered structures have been studied extensively [16,17]. The Earth's strata and general composite materials are two typical examples of layered structures. Although the earliest theoretical discussions can be

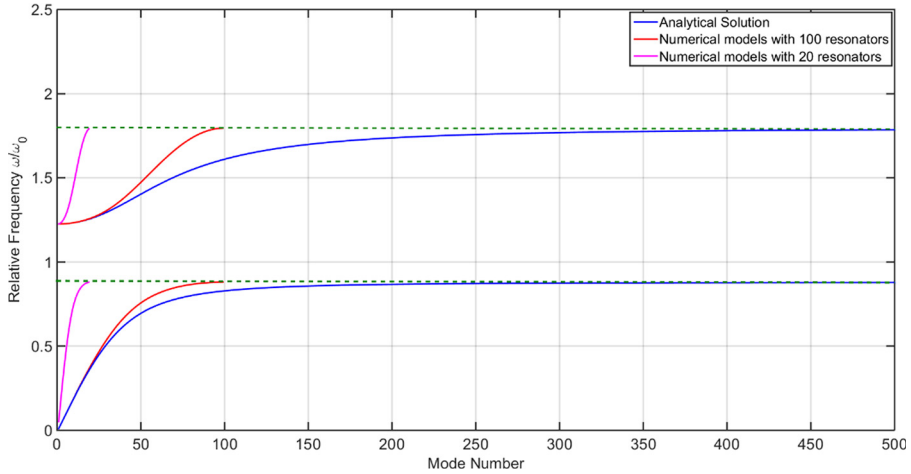


**Fig. 9 Natural frequencies of the elastic metamaterial rod obtained from analytical (Eq. (18)) and numerical models with 100 resonators and 20 resonators**

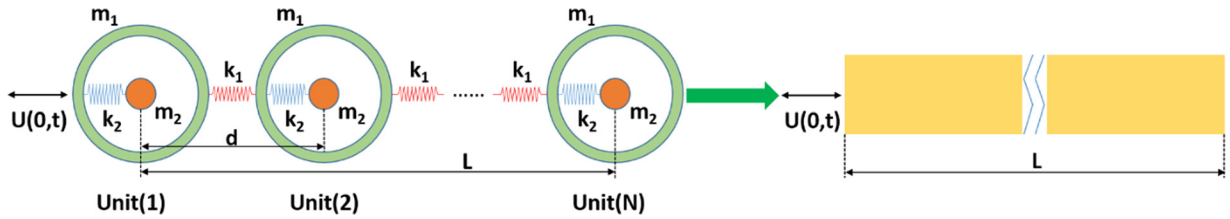


**Fig. 10 Finite lattice model and effective continuum rod with displacement input**

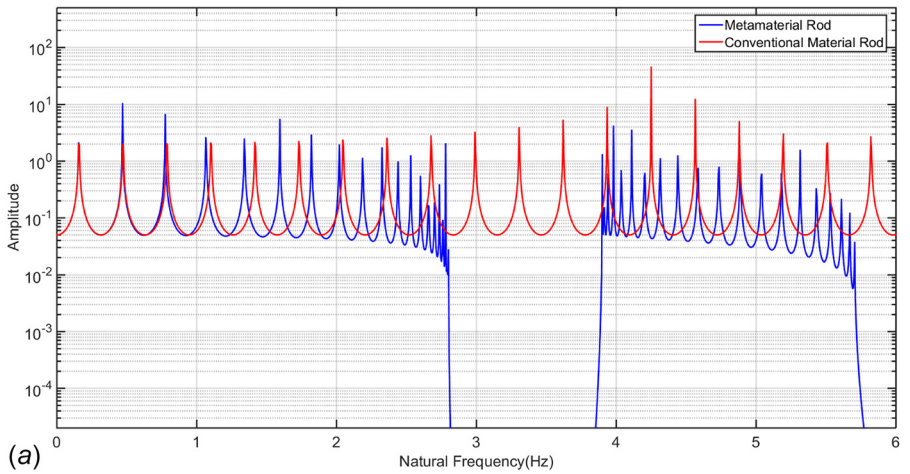


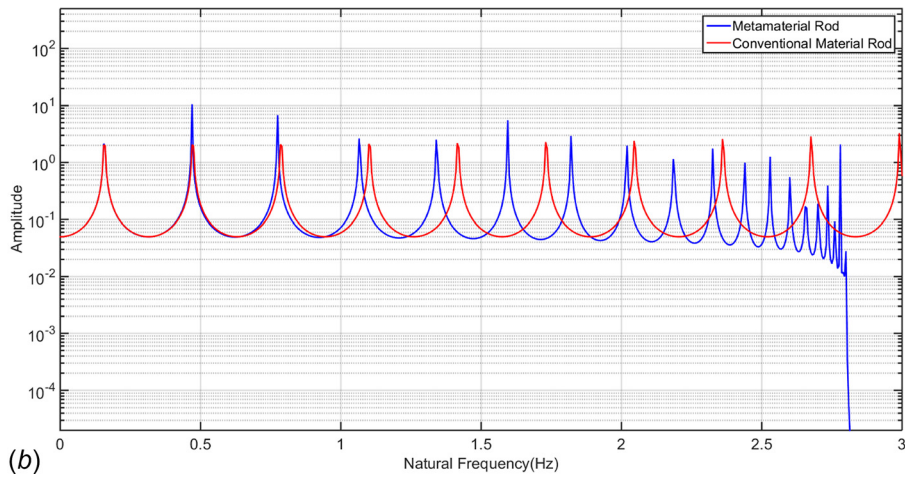


**Fig. 11 Displacement comparison of the remote end in the effective continuum rod and metamaterial-based rod for (*a*) natural frequency distribution comparison and (*b*) natural frequency concentration in the first passing band**

traced back to Thomson's derivation in 1950, conventional materials with their inherent properties limit their applications in multilayered structures.

As discussed in Sec. 2, elastic metamaterials can exhibit arbitrary mass densities or Young's moduli depending on the wave excitation frequency. Thus, elastic metamaterials have an advantage as candidates in layered structures capable of unique wave manipulation properties. In Sec. 4.1, the transfer function is derived for a propagating wave in a layered structure. Then, the resulting transmitted wave amplitude range for the case of a layered structure comprised of elastic metamaterials with a decreasing effective density is studied.

**4.1 Analytical Analysis of Wave Propagation in Finite Layered Structures.** For the layered structure shown in Fig. 12, the governing equation used to describe the wave propagation behavior for a 1D system is given as

$$\frac{\partial}{\partial x}\left(E(x)\cdot\frac{\partial u(x,t)}{\partial x}\right)=\rho(x)\cdot\frac{\partial^2 u(x,t)}{\partial t^2} \tag{21}$$

Similar to Sec. 3.1, based on the spectral approach [20], the displacement solution can be represented by

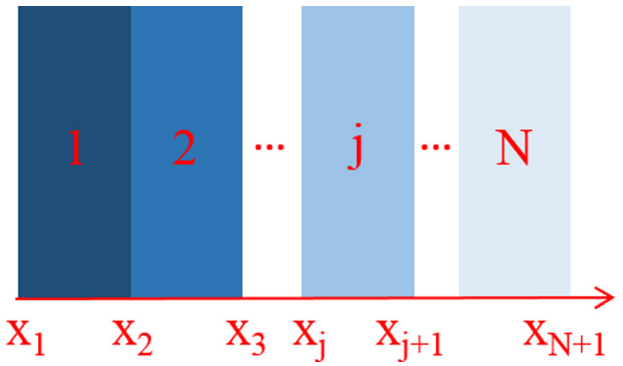


**Fig. 12 Diagram of layered structure**

$$u(x,t) = \hat{u}(x,\omega)e^{i\omega t} \tag{22}$$

For each frequency $\omega$, we define the spectral displacement, $\hat{u}$, in each layer as

$$\hat{u}_j = A_j \cdot e^{-ik_j(x-x_j)} + B_j \cdot e^{ik_j(x-x_j)}, \times \left( j = 1, 2, \ldots, N, k_j = \frac{2\pi}{\lambda_j} = \frac{\omega}{c_j},\ c_j = \sqrt{\frac{E_j}{\rho_j}} \right) \tag{23}$$

The displacement and stress continuity conditions at the interface of two adjacent layers are described by

$$u_j|_{x=x_{j+1}} = u_{j+1}|_{x=x_{j+1}} \tag{24}$$

$$E_j \cdot \frac{\partial u_j}{\partial x}\bigg|_{x=x_{j+1}} = E_{j+1} \cdot \frac{\partial u_j}{\partial x}\bigg|_{x=x_{j+1}} \tag{25}$$

Then, the wave amplitude in each layer can be obtained by transfer function [16,17] $T_j$ as

$$\begin{pmatrix} A_n \\ B_n \end{pmatrix} = \left( \prod_{j=1}^{n-1} T_j \right) \cdot \begin{pmatrix} A_1 \\ B_1 \end{pmatrix}, \quad \text{where}$$
$$T_j = \begin{bmatrix} \frac{1+\alpha_j}{2} e^{-i\omega t_j} & \frac{1-\alpha_j}{2} e^{i\omega t_j} \\ \frac{1-\alpha_j}{2} e^{-i\omega t_j} & \frac{1+\alpha_j}{2} e^{i\omega t_j} \end{bmatrix} \tag{26}$$

where $t_j = (x_{j+1} - x_j)/c_j$, $\alpha_j = Z_j/Z_{j+1}$, and $Z_j = \sqrt{E_j \rho_j}$.

If the last layer is assumed to be infinitely long, the displacement and transfer matrices can be written as

$$\text{Amp}(\hat{u}_1|_{x=x_1}) = 1 = A_1 + B_1 \quad \text{and} \quad B_N = 0 \tag{27}$$

$$T = \left( \prod_{j=1}^{N-1} T_j \right) = \begin{bmatrix} t_{11} & t_{12} \\ t_{21} & t_{22} \end{bmatrix} \tag{28}$$

The final transmitted wave amplitude can then be calculated by

$$A_N = \frac{t_{11}t_{22} - t_{12}t_{21}}{t_{22} - t_{21}} \tag{29}$$

Since the transfer function amplitude, $T$, is a complex matrix, the real amplitude of $A_N$ can be obtained by taking the absolute value as

$$\text{Amp}\,(A_N) = \text{abs}\left( \frac{t_{11}t_{22} - t_{12}t_{21}}{t_{22} - t_{21}} \right) \tag{30}$$

In the following derivation in Sec. 4.1, mathematical induction is used to calculate the range of values for the transmission amplitude $A_N$. For the numerator of Eq. (30), if $N = 2$, it can be found that $t_{11}t_{22} - t_{12}t_{21} = \alpha$. Supposing $N = m \geq 2$, $t'_{11}t'_{22} - t'_{12}t'_{21} = \alpha^{m-1}$ and $\alpha_1 = \alpha_2 = \ldots = \alpha$, then for $N = m + 1$, the transmission amplitude transfer function can be expressed as

$$T = \begin{bmatrix} \frac{1+\alpha}{2} e^{-i\omega t_m} & \frac{1-\alpha}{2} e^{i\omega t_m} \\ \frac{1-\alpha}{2} e^{-i\omega t_m} & \frac{1+\alpha}{2} e^{i\omega t_m} \end{bmatrix} \cdot \begin{bmatrix} t'_{11} & t'_{12} \\ t'_{21} & t'_{22} \end{bmatrix}$$
$$= \begin{bmatrix} \frac{1+\alpha}{2} e^{-i\omega t_m} t'_{11} + \frac{1-\alpha}{2} e^{i\omega t_m} t'_{21} & \frac{1+\alpha}{2} e^{-i\omega t_m} t'_{12} + \frac{1-\alpha}{2} e^{i\omega t_m} t'_{22} \\ \frac{1-\alpha}{2} e^{-i\omega t_m} t'_{11} + \frac{1+\alpha}{2} e^{i\omega t_m} t'_{21} & \frac{1-\alpha}{2} e^{-i\omega t_m} t'_{12} + \frac{1+\alpha}{2} e^{i\omega t_m} t'_{22} \end{bmatrix} \tag{31}$$

$$\Rightarrow t_{11}t_{22} - t_{12}t_{21} = \left( \left( \frac{1+\alpha}{2} \right)^2 - \left( \frac{1-\alpha}{2} \right)^2 \right) \cdot \left( t'_{11}t'_{22} - t'_{12}t'_{21} \right) = \alpha^m \tag{32}$$

Based on Eq. (32), it is clear that for the numerator $t_{11}t_{22} - t_{12}t_{21} = \alpha^{N-1}$.

For the denominator, it can also be derived that its absolute value has a range given by

$$\text{abs}\left( \frac{1}{t_{22} - t_{21}} \right) \in \left[ \frac{1}{\alpha^{N-1}}, 1 \right] \tag{33}$$

where the maximum value is reached when, $\omega t_1 = ((2m+1)\pi)/2$, $(m = 0, 1, \ldots)$ and $\omega t_j = p\pi$, $(p = 1, 2, \ldots, j = 2, 3, \ldots, n)$; while the minimum value $(1/\alpha^{N-1})$ is reached when $\omega t_1 = m\pi$, $(m = 0, 1, \ldots)$ and $\omega t_j = p\pi$, $(p = 1, 2, \ldots, j = 2, 3, \ldots, n)$.

Combining the numerator and denominator components, the amplitude $A_N$ can be obtained as

$$\text{Amp}\,(A_N) = \text{abs}\left( \frac{t_{11}t_{22} - t_{12}t_{21}}{t_{22} - t_{21}} \right) = \text{abs}\left( \frac{\alpha^{N-1}}{t_{22} - t_{21}} \right) \in \left[ 1, \alpha^{N-1} \right] \tag{34}$$

In contrast to the input displacement, for $N$ layers, the stress input is written in the form

$$\text{Amp}\,(\hat{\sigma}_i^1) = \text{Amp}\left( -A_1 E_1 \cdot \frac{\omega}{c_1} i \cdot e^{-\frac{i\omega}{c_1}(x - x_1)} \right) = 1 \tag{35}$$

where $\hat{\sigma}_i^1$ represents the input stress at the first layer. The ratio of the amplitude for the final transmitted stress in the $N$th layer to the unit input stress can then be expressed as

$$\frac{\text{Amp}(\hat{\sigma}_t^N)}{\text{Amp}(\hat{\sigma}_i^1)} = \text{abs}\left( \frac{A_N \sqrt{E_N \rho_N}}{A_1 \sqrt{E_1 \rho_1}} \right) \tag{36}$$

Following the same Mathematical Induction derivation steps used for the displacement boundary conditions and the same symbolic definitions, the range of values for the ratio of $A_N/A_1$ can be obtained as

$$\text{abs}\left( \frac{A_N}{A_1} \right) \in \left[ 1, \alpha^{N-1} \right], \quad \text{and} \quad \frac{\sqrt{E_N \rho_N}}{\sqrt{E_1 \rho_1}} = \frac{1}{\alpha^{N-1}} \tag{37}$$

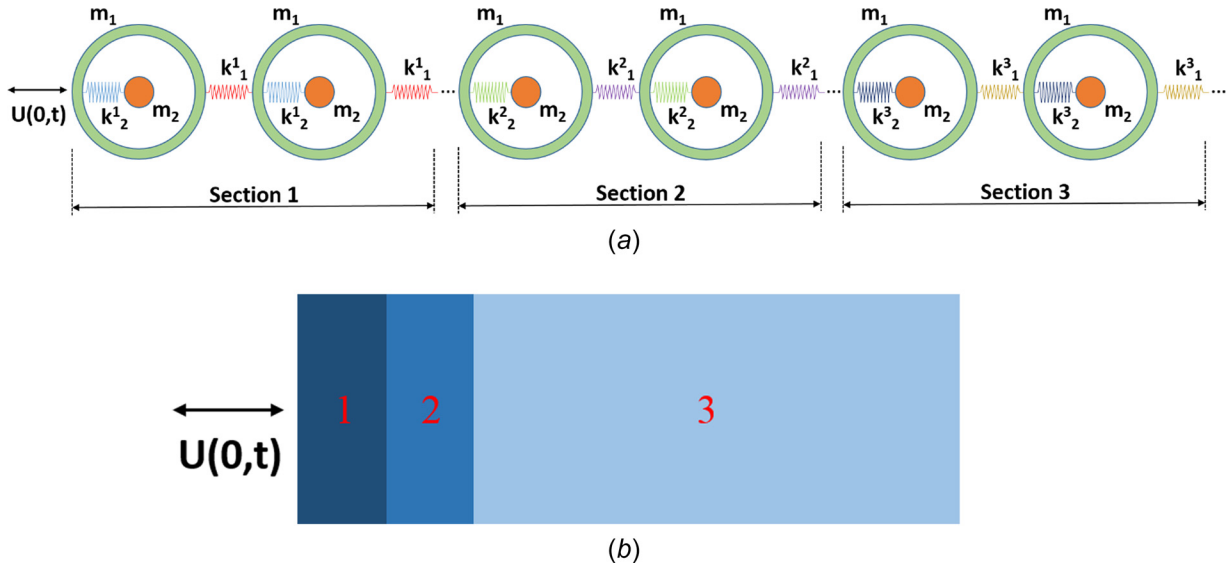


**Fig. 13 (*a*) Three section mass-in-mass lattice model with unit displacement input and (*b*) three section effective continuum model with unit displacement input**

where the ratio of the final transmitted stress to the unit input stress is written as

$$\frac{\mathrm{Amp}\left(\hat{\sigma}_t^N\right)}{\mathrm{Amp}\left(\hat{\sigma}_i^1\right)} \in \left[\frac{1}{\alpha^{N-1}}, 1\right] \tag{38}$$

The minimum value, $1/\alpha^{N-1}$, is reached when $\omega t_1 = ((2m+1)\pi)/2$, $(m=0,1,\ldots)$ and $\omega t_j = p\pi$, $(p=1,2,\ldots, j=2,3,\ldots,n)$, while the maximum value is reached when $\omega t_1 = m\pi$, $(m=0,1,\ldots)$ and $\omega t_j = p\pi$, $(p=1,2,\ldots, j=2,3,\ldots,n)$.

Comparing the maximum and minimum conditions with those of the transmitted wave displacement amplitude, when the increased final transmitted wave displacement amplitude reaches its maximum value, the reduced stress amplitude reaches a minimum value. Furthermore, both values are controlled by the constant adjacent impedance rate "$\alpha$".

**4.2 Numerical Simulation of Wave Propagation in a Finite-Layered Metamaterial Structure.** To verify the maximum value of Amp ($A_N$) obtained from Eq. (30), the mass-in-mass lattice model and its effective continuum model are established with the finite element method software ABAQUS (shown in Fig. 13). The model consists of three sections where the third section is designed to be sufficiently long to avoid the wave reflection from the right end boundary. According to Eqs. (7) and (11), the effective density and effective Young's modulus of each section can be obtained from Eq. (39) as

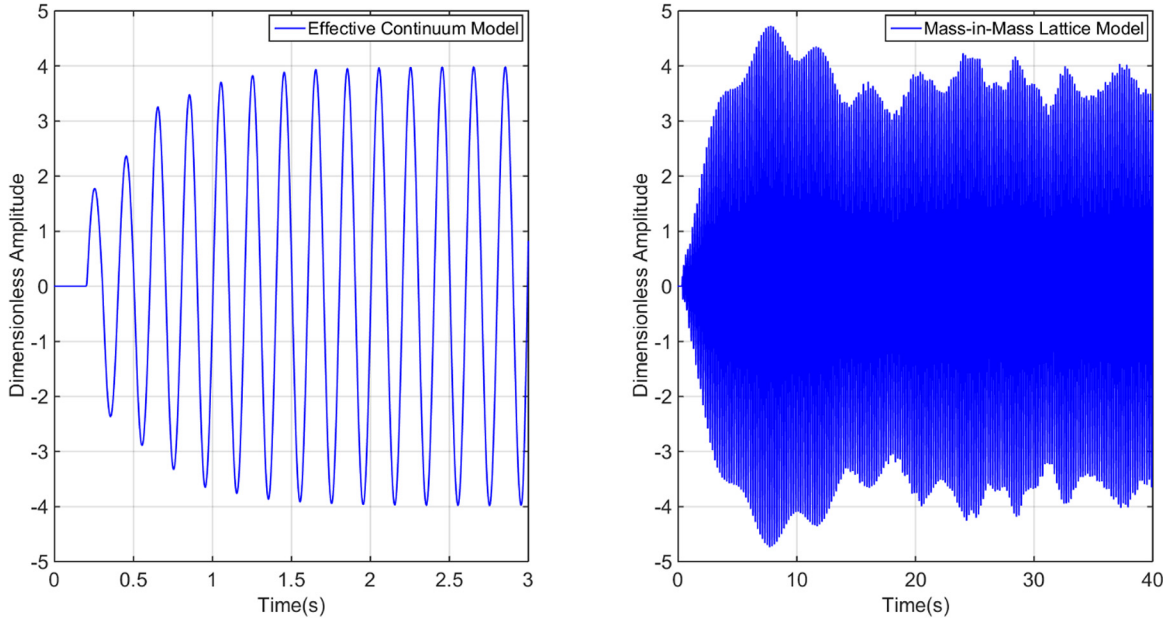


**Fig. 14 Transmitted wave time history (*a*) effective continuum model and (*b*) mass-in-mass lattice model**


(*a*)

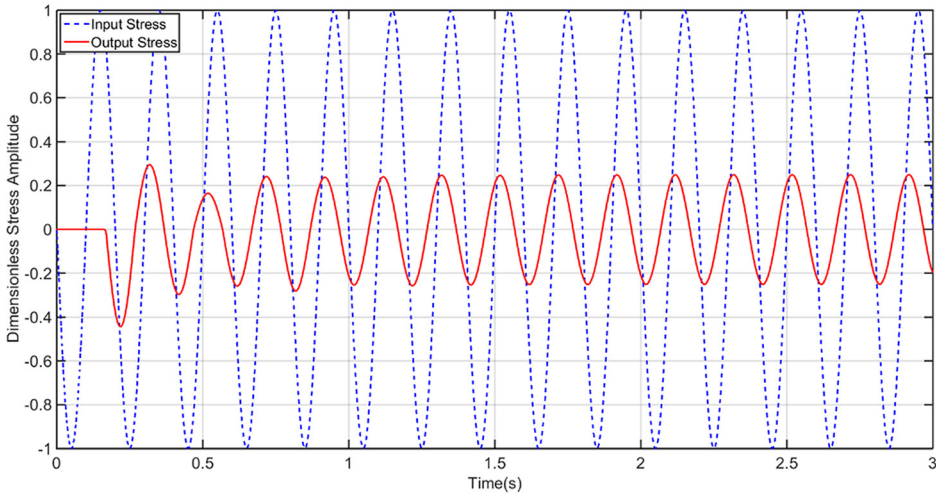


(*b*)

**Fig. 15 (*a*) Three section effective continuum model with unit force input and (*b*) time history comparison for input stress (dashed line) and transmitted stress (solid line)**

$$\rho_{\text{eff}} = \frac{(m_1 + m_2)k_2 - m_1 m_2 \omega^2}{(k_2 - m_2\omega^2)dS} \tag{39a}$$

$$E_{\text{eff}} = \frac{k_1 d}{S} - \frac{(m_1 + m_2)k_2 d\omega^2 - m_1 m_2 d\omega^4}{4S(k_2 - m_2\omega^2)} \tag{39b}$$

To simplify the design, two of the four parameters, $m_1$, $m_2$, $k_1$ and $k_2$, can be controlled to modify the effective material properties of each section. Here, taking $k_1$ and $k_2$ as the control variables, and giving all sections the same values of $m_1 = 24\,\text{kg}$ and $m_2 = 40\,\text{kg}$, and rewriting Eq. (39), $k_1$ and $k_2$ for each section can be obtained from Eq. (40) as

$$k_1 = \frac{E_{\text{eff}} S}{d} + \frac{\rho_{\text{eff}} dS\omega^2}{4} \tag{40a}$$

$$k_2 = \frac{m_2\omega^2(m_1 - \rho_{\text{eff}} dS)}{m_1 + m_2 - \rho_{\text{eff}} dS} \tag{40b}$$

Considering the unit cell cross-sectional area ($S = 1\,\text{m}^2$) and the periodical spacing between each unit cell to be $d = 1$ m, to make the adjacent impedance rate $\alpha = 2$ at the frequency $f = 5\,\text{Hz}$, the effective density and effective Young's modulus are chosen as: $\rho^1_{\text{eff}} = 16\,\text{kg/m}^3$, $E^1_{\text{eff}} = 640{,}000\,\text{Pa}$, for the first section; $\rho^2_{\text{eff}} = 4\,\text{kg/m}^3$, $E^2_{\text{eff}} = 640{,}000\,\text{Pa}$, for the second section; $\rho^3_{\text{eff}} = 1\,\text{kg/m}^3$, $E^3_{\text{eff}} = 640{,}000\,\text{Pa}$, for the third section. Based on Eq. (40), $k_1$ and $k_2$ can be obtained as: $k^1_1 = 643{,}947$ N/m, $k^1_2 = 6579.7$ N/m, for the first section; $k^2_1 = 640{,}987$ N/m, $k^2_2 = 13{,}159.5$ N/m, for the second section; and $k^3_1 = 640{,}247$ N/m, $k^3_2 = 14{,}412.8$ N/m, for the third section. In addition, to satisfy the condition of the maximum value of $\text{Amp}(A_N)$, we set $\omega t_1 = \pi/2$ and $\omega t_2 = \pi$, and the lengths of first two sections can be calculated as $L_1 = 10$ m and $L_2 = 40$ m.

Figure 14 illustrates the time history of the transmitted wave amplitude for the mass-in-mass lattice and the effective continuum model. It is easily observed that the final transmitted wave amplitude of the effective continuum model is amplified as much as 400%, which is the exact maximum value, $\alpha^2$, predicted by Eq. (34). It is also noted that, for the mass-in-mass model (Fig. 14(*b*)), the transmitted wave amplitude fluctuates between $+4$ and $-4$, which is due to the inner mass-spring system. Furthermore, compared to the effective continuum model, the wave amplitude in the mass-in-mass model takes a much longer time to reach a steady-state. This phenomenon is caused by the dispersive characteristics in the mass-in-mass lattice model, which reduces the velocity of the wave-front of the imperfect harmonic input wave. Since the effective continuum model can reach the steady-state wave amplitude of the mass-in-mass lattice model quickly and accurately, the effective continuum model is adopted to verify the analytical solution in Sec. 4.1.

To verify the minimum transmitted stress value obtained from Eq. (38), the unit displacement input is replaced by a unit force input (shown in Fig. 15(*a*)) with the same three sections in the effective continuum model. Figure 15(*b*) compares the time

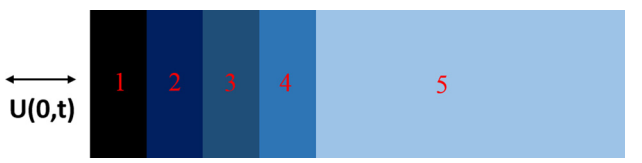


**Fig. 16 Five section effective continuum model with unit displacement input**

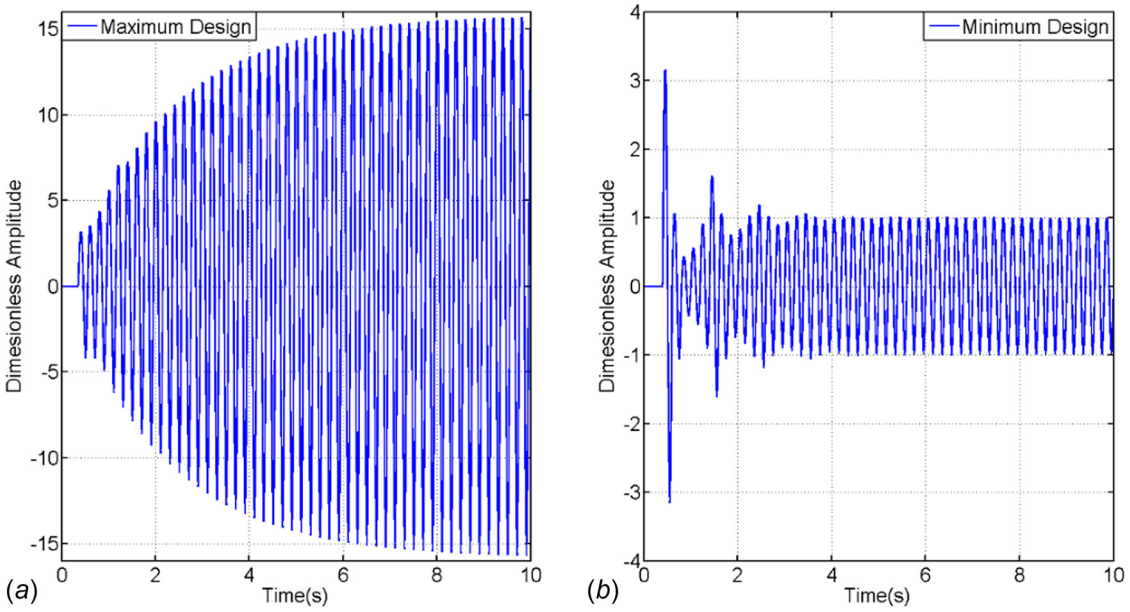


**Fig. 17 Transmitted wave time history for the (*a*) maximum design and (*b*) minimum design**

history of the input stress with the final transmitted stress where it is clear that the input stress amplitude has been reduced by roughly 75%, which matches the minimum value, $1/\alpha^2$, predicted by Eq. (38).

To verify the solution given by Eq. (34), Fig. 16 shows a five-section conventional continuum model with unit displacement input. The mass densities and Young's Moduli for the conventional solids are $\rho_1 = 64\,\text{kg/m}^3$, $\rho_2 = 16\,\text{kg/m}^3$, $\rho_3 = 4\,\text{kg/m}^3$, $\rho_4 = 1\,\text{kg/m}^3$, $\rho_5 = 0.25\,\text{kg/m}^3$, $E_1 = E_2 = E_3 = E_4 = E_5 = 640{,}000\,\text{Pa}$. To satisfy the condition for reaching the maximum or minimum value of Amp ($A_N$), the lengths of the first four sections can be calculated as: $L_1 = 5$ m, $L_2 = 20$ m, $L_3 = 40$ m, $L_4 = 80$ m (maximum design); $L_1 = 10\,\text{m}, L_2 = 20\,\text{m}, L_3 = 40\,\text{m}, L_4 = 80\,\text{m}$ (minimum design).

Figure 17 shows the transmitted wave time history for the maximum and minimum transmission amplitude designs, respectively. Although the transient wave time histories are different for the initial time domain, the two steady-state wave amplitudes (Figs. 17(*a*) and 17(*b*)) match the maximum and minimum values as predicted by Eq. (34). Physically, this phenomenon is due to the mode control in each section by elastic metamaterials.

## 5 Conclusion

This paper is focused on the analysis of finite elastic metamaterial structures with frequency-dependent mechanical properties, and main attention is paid on the frequency application from band gap to the passing band. Based on a simplified mass-in-mass metamaterial lattice model, the equations for the frequency-dependent mass density and Young's modulus for its equivalent continuum model are derived. By utilizing the frequency-dependent mechanical properties, the vibration response of the finite elastic metamaterial rod is studied. It is found that no natural resonance frequency can exist within the band gap frequency region of the corresponding metamaterial. In addition, due to the variation of the effective mass density and Young's modulus, the natural resonance frequency distribution of the rod is changed, especially in the frequency region close to the local resonance frequency of the unit cells in the structure. Finally, wave propagation behavior in layered structures made of elastic metamaterials is investigated. Based on the spectral approach, the general wave amplitude transfer function is derived for wave propagation in the layered structures. The final transmitted wave amplitude range of the layered elastic metamaterial structure with decreasing density is obtained using the mathematical induction method. It is found that when the final transmitted wave displacement amplitude reaches its maximum value, the reduced stress amplitude reaches its minimum value. Subsequently, the amplitudes can be controlled by the impedance mismatch of the adjacent layers in the layered elastic metamaterial structure.

## Funding Data


- Air Force Office of Scientific Research (Grant No. FA9550-15-1-0016).
- Defense Threat Reduction Agency (Grant No. DTRA1-12-1-0047).


## References


[1] Liu, Z., Zhang, X., Mao, Y., Zhu, Y. Y., Yang, Z., Chan, C. T., and Sheng, P., 2000, "Locally Resonant Sonic Materials," Science, **289**(5485), pp. 1734–1736.

[2] Milton, G. W., and Willis, J. R., 2007, "On Modifications of Newton's Second Law and Linear Continuum Elastodynamics," Proc. R. Soc. A, **463**(63), pp. 855–880.

[3] Huang, H. H., Sun, C. T., and Huang, G. L., 2009, "On the Negative Effective Mass Density in Acoustic Metamaterials," Int. J. Eng. Sci., **47**(4), pp. 610–617.

[4] Huang, H. H., and Sun, C. T., 2009, "Wave Attenuation Mechanism in an Acoustic Metamaterial With Negative Effective Mass Density," New J. Phys., **11**(1), p. 013003.

[5] Huang, G. L., and Sun, C. T., 2010, "Band Gaps in a Multiresonator Acoustic Metamaterial," ASME J. Vib. Acoust., **132**(32), p. 031003.

[6] Liu, Y., Shen, X., Su, X., and Sun, C. T., 2016, "Elastic Metamaterials With Low-Frequency Passbands Based on Lattice System With On-Site Potential," ASME J. Vib. Acoust., **138**(2), p. 21011.

[7] Lee, S. H., Park, C. M., Seo, Y. M., Wang, Z. G., and Kim, C. K., 2010, "Composite Acoustic Medium With Simultaneously Negative Density and Modulus," Phys. Rev. Lett., **104**(5), p. 054301.

[8] Liu, X. N., Hu, G. K., Huang, G. L., and Sun, C. T., 2011, "An Elastic Metamaterial With Simultaneously Negative Mass Density and Bulk Modulus," Appl. Phys. Lett., **98**(25), p. 251907.

[9] Jing, Y., Xu, J., and Fang, N. X., 2012, "Numerical Study of a Near-Zero-Index Acoustic Metamaterial," Phys. Lett. Sect. A, **376**(45), pp. 2834–2837.

[10] Graciá-Salgado, R., García-Chocano, V. M., Torrent, D., and Sánchez-Dehesa, J., 2013, "Negative Mass Density and $\rho$-Near-Zero Quasi-Two-Dimensional Metamaterials: Design and Applications," Phys. Rev. B, **88**(22), p. 224305.

[11] Park, J. J., Lee, K. J. B., Wright, O. B., Jung, M. K., and Lee, S. H., 2013, "Giant Acoustic Concentration by Extraordinary Transmission in Zero-Mass Metamaterials," Phys. Rev. Lett., **110**(24), p. 244302.

[12] Wei, Q., Cheng, Y., and Liu, X. J., 2013, "Acoustic Total Transmission and Total Reflection in Zero-Index Metamaterials With Defects," Appl. Phys. Lett., **102**(17), p. 174104.

[13] Cummer, S. A., Christensen, J. C., and Alu, A., 2016, "Controlling Sound With Acoustic Metamaterials," Nat. Rev. Mater., **1**(3), p. 16001.

[14] Qian, W., Yu, Z., Wang, X., Lai, Y., and Yellen, B. B., 2016, "Elastic Metamaterial Beam With Remotely Tunable Stiffness," J. Appl. Phys., **119**(5), p. 055102.

[15] Huang, L.-Z., Xiao, Y., Wen, J. H., Yang, H. B., and Wen, X. S., 2016, "Analysis of Underwater Decoupling Properties of a Locally Resonant Acoustic Metamaterial Coating," Chin. Phys. B, **25**(2), p. 24302.
[16] Luo, X., 2007, "Development of Layered Elastic Stress Wave Attenuators for Mitigating Impulsive Loadings," Ph.D. thesis, University at Buffalo, Buffalo, NY.
[17] Luo, X., Aref, A. J., and Dargush, G. F., 2009, "Analysis and Optimal Design of Layered Structures Subjected to Impulsive Loading," Comput. Struct., **87**(9–10), pp. 543–551.
[18] Thomson, W. T., 1950, "Transmission of Elastic Waves Through a Stratified Solid Medium," J. Appl. Phys., **21**(2), pp. 89–93.
[19] Srivastava, A., and Willis, J. R., 2017, "Evanescent Wave Boundary Layers in Metamaterials and Sidestepping Them Through a Variational Approach," Proc. R. Soc. A, **473**(73), p. 20160765.
[20] Doyle, J. F., 1997, *Wave Propagation in Structures Spectral Analysis Using Fast Discrete Fourier Transforms*, Springer, New York.
[21] Samadhiya, R., Mukherjee, A., and Schmauder, S., 2006, "Characterization of Discretely Graded Materials Using Acoustic Wave Propagation," Comput. Mater. Sci., **37**(1–2), pp. 20–28.
[22] Liu, Y., Su, X., and Sun, C. T., 2015, "Broadband Elastic Metamaterial With Single Negativity by Mimicking Lattice Systems," J. Mech. Phys. Solids, **74**(40), pp. 158–174.